

miR-520d-3p/MIG-7 axis regulates vasculogenic mimicry formation and metastasis in osteosarcoma

Nan YAO^{1,2,*}, Jing ZHOU^{1,2}, Jie SONG^{1,2}, Yantao JIANG³, Jian ZHANG^{1,2}

¹Affiliated Hospital of Integrated Traditional Chinese and Western Medicine, Nanjing University of Chinese Medicine, Nanjing, Jiangsu, China; ²Laboratory of Translational Medicine, Jiangsu Province Academy of Traditional Chinese Medicine, Nanjing, Jiangsu, China; ³Department of Medical Oncology, Suzhou Traditional Chinese Medicine Hospital Affiliated to Nanjing University of Chinese Medicine, Suzhou, Jiangsu, China

*Correspondence: yaonan_nj@163.com

Received November 28, 2021 / Accepted March 10, 2022

Vasculogenic mimicry (VM) refers to a novel mode of tumor microcirculation, which provides an escape route for tumor metastasis, and thereby correlates with a poor prognosis. We previously reported MIG-7 plays a pivotal role in osteosarcoma (OS) VM. However, the precise mechanism of MIG-7 in regulating OS VM remains to be elucidated. The expression levels of miR-520d-3p and MIG-7 were measured in OS cell lines. The effects of the miR-520d-3p/MIG-7 axis were investigated by *in vitro* functional assays. An orthotopic xenograft model was established to assess the role of the miR-520d-3p/MIG-7 axis in OS cells *in vivo*. Phalloidin staining, western blot, immunohistochemistry, ELISA assays were carried out to explore the molecular events that were involved in the miR-520d-3p/MIG-7 axis-mediated VM formation. The miR-520d-3p expression level was inversely correlated with MIG-7 in these cell lines. miR-520d-3p overexpression suppressed the proliferation, migration, invasion, VM, and promotes the adhesion of OS cells *in vitro*. miR-520d-3p could directly bind to the 3'-UTR of MIG-7 and regulated MIG-7 expression, which led to impaired lamellipodia and filopodia formation and inactivation of the PI3K/MMPs/Ln-5γ2 signaling pathway. The anti-metastatic and anti-VM effects of miR-520d-3p were confirmed *in vivo*. Our findings suggest miR-520d-3p acts as a tumor suppressor by inhibiting VM formation in OS via targeting MIG-7.

Key words: osteosarcoma, vasculogenic mimicry, miR-520d-3p, MIG-7, metastasis

Osteosarcoma (OS) is the most common bone malignancy, which predominantly arises in children and adolescents [1]. Despite OS has a relatively low incidence, its high tendency to form lung metastases contributes to high mortality and poor prognosis [2]. Although neoadjuvant chemotherapy regimens have extended the survival rate of OS patients with local disease from less than 20% to approximately 65%, effective treatment for patients with metastatic disease has yet to be defined [3]. It causes the 5-year survival rate to be as low as 10–30% for decades in terms of this subgroup of OS patients [4]. Hence arises the urgent need for better understanding molecular mechanisms underlying OS metastasis and developing novel therapeutics.

It is a well-known fact that blood vessels are essential for tumor growth and metastasis [5]. Besides angiogenesis and vasculogenesis, vasculogenic mimicry (VM) is a new avenue of tumor cells exploited to recruit blood vessels [6]. It describes a process by which tumor cells mimic endothelial cells and get involved in the formation of the blood vessel wall [7]. Because the wall of VM consisted exclusively of

tumor cells, it provides a route for a tumor cell to expose directly to circulation, thereby enhancing the risk of developing distant metastasis. Therefore, VM has been linked to high tumor grade, decreased life span, and increased mortality in varieties of human malignancies [8]. We previously reported that VM has been found in OS and involved in OS metastasis and poor prognosis [9]. Despite its clinical significance, the molecular events mediating VM formation in OS remain unclear.

Migration-inducing gene 7 (MIG-7) is a cysteine-rich protein, which is limited to metastatic tumors but undetectable in normal tissues [10]. Recently, accumulated evidence has shown that MIG-7 plays an oncogenic role in numerous tumors by promoting tumor metastasis through increased invasiveness and VM [11]. In melanoma, MIG-7 is highly expressed in metastatic melanoma cell lines, which could form VM structures compared with low expression in poorly metastatic ones that could not form VM [12]. Downregulation of MIG-7 inhibited the process of VM formation and tumor dissemination in endometrial carcinoma [13]. In

addition, our previous study demonstrated a positive correlation between MIG-7 level with VM formation and poor prognosis in primary OS patients. Accordingly, MIG-7 knockdown exhibited anti-VM and anti-OS effects [14]. Previous studies showed that the cleavage of Laminin-5 γ 2 (Ln-5 γ 2) into its chain fragmentation is needed for VM of highly malignant tumor cells [15]. And MMPs are identified as the upstream regulators in this cleavage event [16]. Inhibition of PI3K could inhibit VM by reducing MMPs and blocking the Ln-5 γ 2 cleavage [17]. MIG-7 protein expression co-localizes with Ln-5 γ 2 fragments in patterned networks in lymph nodes from xenograft nude mice [12], implying that disordered MIG-7 might be involved in VM formation by the PI3K/MMPs/Ln-5 γ 2 signaling pathway. However, the mechanism mediating the aberrant expression of MIG-7 in OS and downstream effectors of MIG-7 are poorly understood.

MicroRNAs, a family of 19–25 nucleotide-long noncoding RNAs, participate in almost every cancer-related process including VM [18–20]. By binding to the complementary sequences in the 3' untranslated region (3'-UTR) of their target gene mRNA, miRNAs repress the corresponding gene expression via mRNA degradation or translation inhibition [21]. To date, miRNAs-based strategy has been proposed as a potential approach for OS treatment [22]. Thus far, little is known about the role of miRNAs in OS VM. Identifying specific miRNA and its target gene in VM may offer a promising target in the development of new therapies for OS.

Herein, we demonstrated an inverse correlation between miR-520d-3p and MIG-7 levels in OS cell lines. miR-520d-3p suppresses VM formation and metastasis of OS cells *in vitro* and *in vivo* by regulating MIG-7 expression. miR-520d-3p directly targeted and downregulated the expression of MIG-7, which led to the reduced invasion and VM phenotype in OS via modulating lamellipodia and filopodia formation and the PI3K/MMPs/Ln-5 γ 2 signaling pathway. These results suggested that miR-520d-3p/MIG-7 axis might serve as a potential therapeutic target for OS.

Materials and methods

Cell culture and transfection. Human fetal osteoblast hFOB1.19 cell line, six human OS cell line HOS, Saos-2, U-2 OS, MG-63, 143B, MNNG/HOS, and HEK293T cell were used in this study. All the cell lines were obtained from ATCC and cultured in appropriate medium (high glucose DMEM for Saos-2, U-2 OS, 143B, and HEK293T; RPMI-1640 for HOS; MEM for MG-63 and MNNG/HOS) supplemented with 10% fetal bovine serum (Thermo Fisher Scientific, Inc., Waltham, MA, USA) at 37°C in a humidified atmosphere of 5% CO₂. hFOB1.19 cell line was grown in a 1:1 mixture of DMEM/F12 supplemented with 10% FBS in 34°C, 5% CO₂ incubator.

The miR-520d-3p mimic, inhibitor, and scrambled negative controls were purchased from GenePharma

(Shanghai, China). miR-520d-3p transfection was conducted at a concentration of 50 nM using Lipofectamine 2000 (Invitrogen, Carlsbad, CA, USA). MIG-7 expression vector was constructed by cloning the open reading frame of MIG-7 (Accession DQ080207) into GV230 vector purchased from GeneChem (Shanghai, China). An empty vector served as the negative control. Twenty-four hours after transfection, the cells were collected for subsequent experiments. LY294002 (20 μ M, Sigma-Aldrich, St. Louis, MO, USA), a specific inhibitor of PI3K, was applied to verify the role of the PI3K/AKT pathway in the miR-520d-3p/MIG-7 axis-mediated VM formation, with DMSO serving as a control.

Cell proliferation assay. Briefly, cells transfected with oligonucleotides or plasmids were plated in 96-well plates and incubated overnight. At different time points, 10 μ l volume of the CCK-8 solution (Keygentec, Nanjing, China) was then added to cells. After 4 h, the absorbance was recorded at a wavelength of 450 nm using a microplate reader (Synergy H1, BioTek, Winooski, VT, USA).

Cell adhesion assay. Cells were seeded in the 96-well plate coated with fibronectin (Sigma-Aldrich, St. Louis, MO, USA) or laminin (Sigma-Aldrich) and incubated for 1 h to allow cells to adhere to the surface. After rinsing with PBS, cells were fixed for 30 min in 4% paraformaldehyde and stained with crystal violet (Beyotime, Shanghai, China) for 15 min. The bound dye was then dissolved with 33% acetic acid. The absorbance was measured at 590 nm using a Synergy H1 microplate reader.

Wound healing assay. A wound gap was created by scratching the cell monolayer with a 200 μ l tip. Plates were photographed at 0 h and 24 h after scratching using an inverted microscope (Primo Vert, Zeiss, Germany). Wound closure is calculated as the closed width of the wound at 24 h relative to the initial wound width using Image pro plus (IPP) software (Media Cybernetics, Silver Spring, MD, USA).

Cell migration and invasion assay. Briefly, cells resuspended in a serum-free medium were seeded in the upper Transwell chamber (Corning, NY, USA) pre-coated with (for invasion assay) or without (for migration assay) Matrigel (BD Biosciences, Bedford, MA). Medium containing 10% FBS was added to the lower chamber. After 24 h (for migration assay) or 48 h (for invasion assay), the penetrating cells were stained with crystal violet and counted under an inverted contrast microscope.

***In vitro* VM assay.** To assess the VM formation *in vitro*, cells were loaded on the surface of pre-coated BD Matrigel. The pictures of tube-like channels were taken and quantified by counting the number of tube connections as reported previously [14].

Phalloidin staining. Cells were grown on coverslips for 24 h, fixed in 4% paraformaldehyde, permeated with TritonX-100, and stained with Rhodamine-Phalloidin (R&D system, Minneapolis, MN, USA). After washing thrice with PBS, the cells were counterstained with DAPI and examined under microscopy (Axio Primo Vert A1, Carl Zeiss, Germany).

ELISA assay. The levels of MMP-2 and MMP-14 in cell culture supernatant were determined using ELISA kits (MultiSciences, Hangzhou, China) according to the manufacturing instruction.

Dual-luciferase reporter assay. The 3'-UTR sequence of MIG-7 containing the wild type or mutant type of predicted miR-520d-3p binding sites were cloned into a pmiGLO-dual-luciferase miRNA target expression vector (GenePharma, Shanghai, China). HEK293T cells were seeded into 48-well plates, co-transfected with miR-520d-3p mimic or mimic control and the corresponding dual-luciferase vectors. After 48 h, luciferase activities were measured by Dual-Luciferase Reporter Assay Kit (Promega, Madison, WI, USA). The ratio of firefly to Renilla luciferase activity was used to normalize the firefly luciferase values.

Western blot analysis. Cells were collected and lysed in RIPA (Beyotime) supplemented with a proteinase inhibitor cocktail (Solarbio, Beijing, China). An equal amount (50 µg) of the protein samples were separated by SDS-PAGE and incubated with the primary antibodies against MIG-7 (1:1000, bs-5781R, Bioss, Woburn, MA, USA), AKT (1:2000, C67E7, CST, Danvers, MA, USA), p-AKT (1:2000, D9E, CST), mTOR (1:1000, 7C10, CST), p-mTOR (1:1000, D9C2, CST), laminin-5γ2 and its fragments (1:1000, D4B5, Chemicon, Temecula, CA, USA) at 4°C overnight, followed by incubating with horseradish peroxidase-labeled secondary antibody (SA00001-1, Proteintech, Wuhan, China). β-actin (1:2000, 66009-1-Ig, Proteintech) was used as an internal control. The bands were visualized by ECL kit (Tanon, Shanghai, China) and quantized by IPP software.

Quantitative RT-PCR analysis. Total RNA was extracted from cells or tissues using Trizol reagent (Invitrogen). After synthesizing cDNAs with a miRNA 1st strand cDNA Synthesis Kit (Vazyme, Nanjing, China), the expression levels of miR-520d-3p were analyzed using miRNA SYBR qPCR Master Mix (Vazyme) on ABI 7500 PCR system (Applied Biosystems, Foster City, CA, USA). U6 was used as the internal control and the expression levels were normalized to those of the internal controls, and fold changes were calculated using the $2^{-\Delta\Delta CT}$ method. All primer sequences are listed in Supplementary Table S1.

In vivo xenograft model. Animal care and experiments were conducted in accordance with the guidelines of the Animal Care and Use Committee of Jiangsu Province Academy of Traditional Chinese Medicine and in compliance with the ARRIVE guidelines. Six-week-old BALB/c nude mice were purchased from Shanghai Lingchang Bio-Tech Co., Ltd. (Certificate no. SCXX (HU) 2018-0003).

The miR-520d-3p overexpression lentivirus was purchased from Genechem (Shanghai, China). Stably infected cell lines were selected by adding 1 µg/ml puromycin (Sigma-Aldrich) for a week. The mice were randomly divided into four groups (n=8 per group) and approximately 5×10^5 cells (in 10 µl of PBS) infected with control lentivirus, miR-520d-3p overexpression lentivirus, MIG-7 overexpression plasmid, or

miR-520d-3p overexpression lentivirus, and MIG-7 overexpression plasmid were orthotopically injected into the medullary cavity of the left proximal tibia, respectively. Leg volumes were measured every 4 days with a caliper and tumor volume was calculated based on the equation: Leg volume = Length \times Width² \times 0.5, Tumor volume = Leg volume on day X - Leg volume on day 0. Time to endpoint was recorded for survival analysis.

In another parallel experiment, all mice were sacrificed at 40 days post-injection. Tumors in the tibia were excised for weight, RNA extraction, hematoxylin and eosin (H&E) staining, and immunostaining. Lungs were also harvested to observe the metastases.

Immunohistochemistry staining. Tissue sections were deparaffinized in xylene and rehydrated in ethanol. After antigen retrieval in sodium citrate buffer, sections were blocked and incubated with primary antibodies, followed by secondary antibodies and diaminobenzidine method to visualize the staining. The primary antibodies used for IHC were as follows: MIG-7 (1:100, bs-5781R, Bioss), p-AKT (1:100, D9E, CST), p-mTOR (1:100, D9C2, CST), MMP-2 (1:200, 10373-2-AP, Proteintech), MMP-14 (1:100, 14552-1-AP, Proteintech). Semi-quantitative scoring of IHC was based on integrated optical density (IOD) values using IPP software [23].

For CD31-PAS double staining, anti-CD31 (1:200, sc-376764, Santa Cruz, CA, USA) antibody was applied to the sections, followed by 0.5% periodic acid solution incubation. The quantification of double staining was performed as previously described [14].

Statistical analysis. Statistical calculations were performed using SPSS package 19.0 (Chicago, IL, USA) and GraphPad Prism version 5.0 (San Diego, CA, USA). Data were expressed as mean \pm SD or as indicated. Comparisons between groups were performed using a one-way ANOVA test. Categorical variables were compared using Fisher's exact test. The correlation among data was analyzed using Pearson's correlation coefficient assay. Survival curves were plotted by the Kaplan-Meier method with a p-value generated from the log-rank test. Differences with p<0.05 were considered statistically significant.

Results

miR-520d-3p is downregulated in human OS cell lines with VM potentials. To further explore the mechanism of dysregulation of MIG-7 in VM formation, we examined the protein levels of MIG-7 and VM formation in six OS cell lines and a normal osteoblast hFOB1.19 cell line. Higher MIG-7 expression level was detected in these OS cell lines than in normal osteoblast cell line (Figure 1C). Moreover, the differential abilities of these cells to form VM channels are also shown in Figures 1A and 1B. Furthermore, increased MIG-7 protein is accompanied by increased VM potentials in OS cell lines. Since miRNAs are highlighted as an impor-

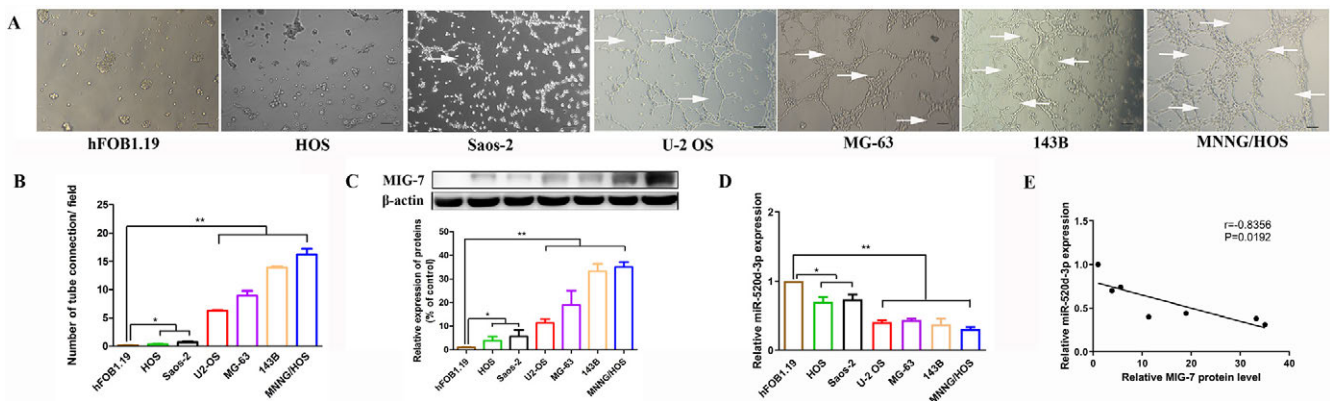


Figure 1. Reduced miR-520d-3p expression was found in OS cell lines with increased VM formation capacities. **A)** Representative image of different VM formation abilities of six OS cell lines and a normal osteoblast hFOB1.19 cell line. Scale bars: 100 μ m. White arrows show VMs formed by OS cells. **B)** Quantitative analyses of VM channels formed by cells. **C)** Comparison of MIG-7 protein in seven cell lines. **D)** qRT-PCR analysis of miR-520d-3p levels in seven cell lines. **E)** Pearson's correlation scatter plot of the relative changes of miR-520d-3p and MIG-7 protein levels in seven cell lines. Values are expressed as mean \pm SD (n=3). * p <0.05, ** p <0.01

tant gene regulatory mechanism in OS, we hypothesized that MIG-7 may be regulated by miRNA in OS. Because miRNAs and their targets mRNAs often exhibit opposite expression patterns and functions, we tried to identify miRNAs that act as tumor suppressor miRNAs. First, bioinformatics algorithms, miRanda [24] and PITA [25] were used to predict miRNAs that target MIG-7. Among the top 10 miRNAs with the lowest free energy, miR-520d-3p has been reported as a tumor suppressor in various types of tumors [26, 27]. However, whether miR-520d-3p is involved in OS development remains unclear. We next found that miR-520d-3p expression levels were obviously decreased in OS cell lines with VM potentials compared with those in normal osteoblast cell line (Figure 1D). Furthermore, miR-520d-3p expression level was inversely correlated with MIG-7 protein levels in these cell lines, suggesting MIG-7 is a potential target of miR-520d-3p (Figure 1E).

miR-520d-3p inhibits OS cell proliferation, migration, invasion, VM, and increases cell adhesion *in vitro*. miR-520d-3p was significantly overexpressed or knocked down in 143B and MG-63 cells as shown in Supplementary Figures S1A and S1B. Compared with the control group, miR-520d-3p mimic delayed cell proliferation in 143B and MG-63 cells, whereas the miR-520d-3p inhibitor increased cell proliferation (Figure 2A). Cells with increased miR-520d-3p levels had a higher adhesive capacity than those in control cells, and decreased miR-520d-3p levels led to lower adhesive capacity (Figure 2B). The migration and invasion capabilities were decreased in cells with overexpression of miR-520d-3p. Conversely, inhibition of miR-520d-3p promoted both capabilities (Figures 2C–2E). Overexpression of miR-520d-3p markedly disrupted tubular networks formation in OS cells; in contrast, miR-520d-3p inhibition promoted VM formation (Figure 2F). Together, these data suggest that miR-520d-3p can inhibit the prolif-

eration, migration, invasion, VM formation, and increase the adhesion of OS cells *in vitro*.

MIG-7 is a direct target of miR-520d-3p. As anticipated, MIG-7 protein levels were dramatically downregulated upon miR-520d-3p overexpression and upregulated upon knock-down of miR-520d-3p in 143B and MG-63 cells (Figures 3A, 3B). Luciferase activity was reduced by approximately 50% by miR-520d-3p mimic in cells co-transfected with MIG7-3'-UTR-WT (Figure 3C). The luciferase activities remained unchanged in cells with the mutated reporter (Figure 3D). Taken together, these data suggest that miR-520d-3p could directly regulate MIG-7 by targeting its 3'-UTR.

miR-520d-3p suppresses OS cell growth, migration, invasion, VM formation, and promotes cell adhesion through targeting MIG-7. To further confirm if the impact of miR-520d-3p in modulating OS's behavior relied on MIG-7, rescue experiments were conducted in which the MIG-7 overexpression vector was used to restore MIG-7 expression inhibited by miR-92b-3p mimic. Restoration of MIG-7 greatly attenuated miR-520d-3p-mediated tumor inhibitory effect, as shown by increased proliferation (Figures 4A, 4B), migration (Figures 4A, 4D, 4E), invasion (Figures 4A, 4F), VM channels (Figures 4A, 4G), and decreased adhesion (Figures 4A, 4C). These data revealed that miR-520d-3p inhibited OS proliferation, migration, invasion, VM formation, and promoted adhesion through targeting MIG-7.

The miR-520d-3p/MIG-7 axis regulates lamellipodia and filopodia formation and PI3K/MMPS/Ln-5 γ 2 pathway to modulate VM in OS. In the process of VM formation, tumor cells interact with each other through cellular protrusions including lamellipodia and filopodia, ultimately lining up and forming tubular networks [28]. Results showed that overexpression of miR-520d-3p in 143B and MG-63 cells inhibited lamellipodia and filopodia formation (Figure 5A).

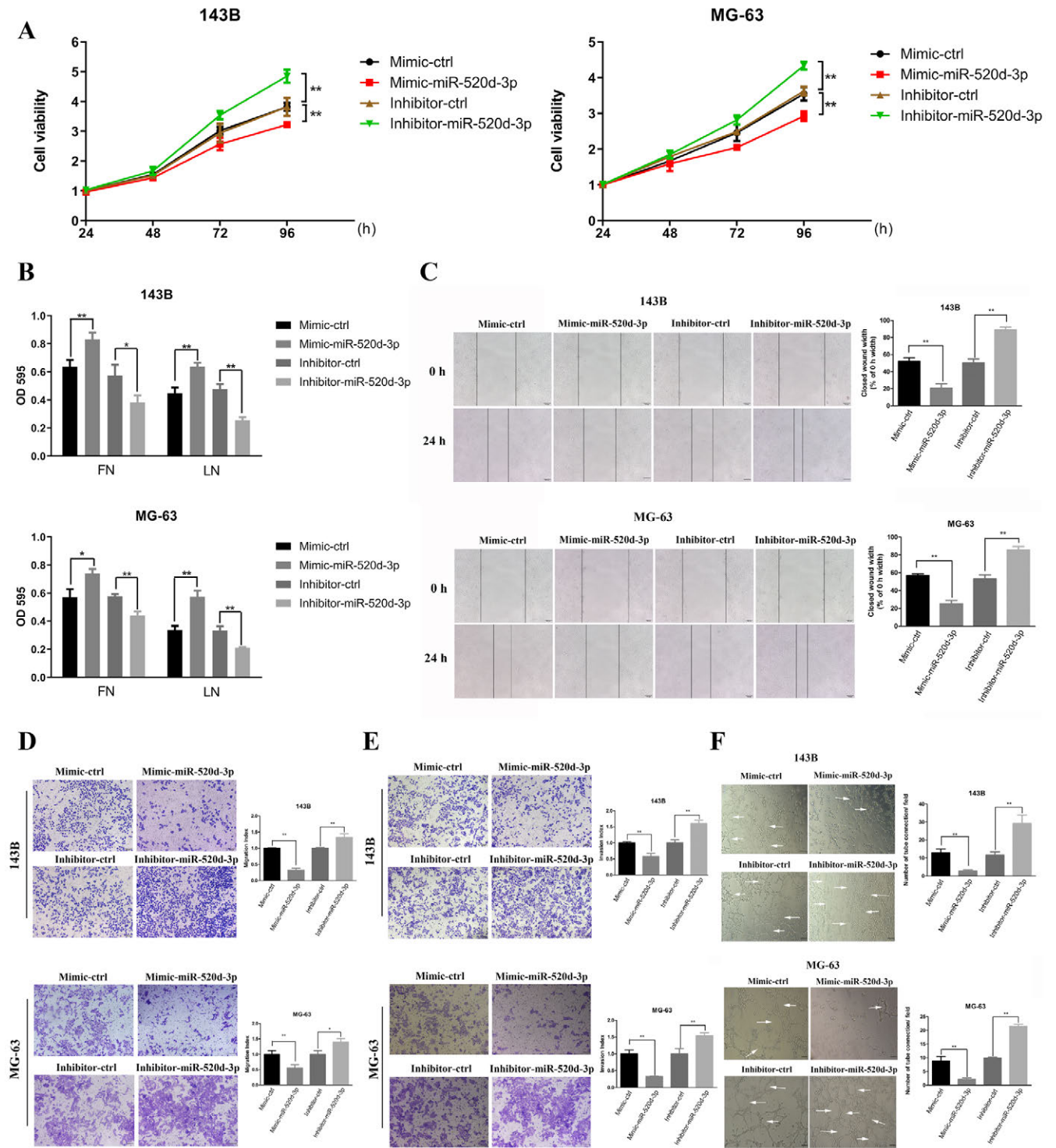


Figure 2. miR-520d-3p inhibits OS cell growth, adhesion, migration, invasion, VM, and promotes cell adhesion *in vitro*. 143B and MG-63 cells were transfected with miR-520d-3p mimic, inhibitor, or negative control. CCK-8 (A), cell adhesion (B), wound-healing (C), Transwell (D-E), and tube formation (F) assays were performed to evaluate the effect of miR-520d-3p alteration on cells. Values are expressed as mean \pm SD (n=3). White arrows show VMs formed by OS cells. Scale bars: 100 μ m. *p<0.05, **p<0.01

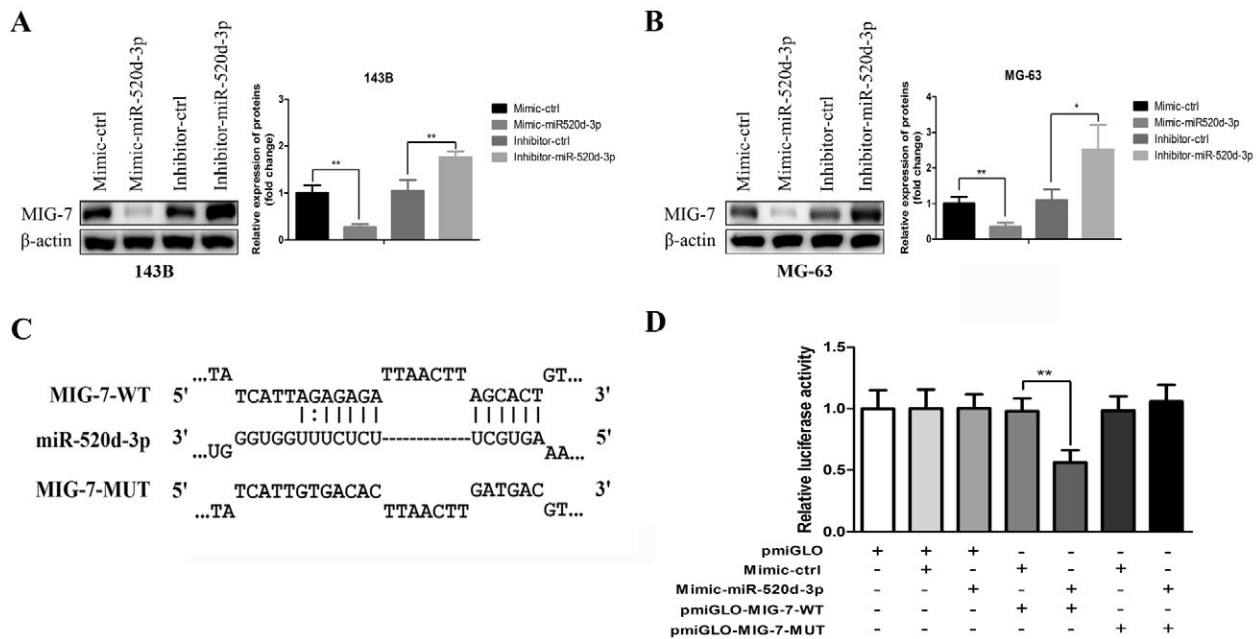


Figure 3. miR-520d-3p directly targeted the 3'-UTR of MIG-7 to suppress its expression. Western blot analyses of MIG-7 expression levels in 143B (A) and MG-63 cells (B) transfected with miR-520d-3p mimic, inhibitor, or negative control. C) Schematic descriptions of the putative miR-520d-3p binding site (wild type, WT) in the 3'-UTR of MIG-7 mRNA, and the mutant binding site (mutant type, MUT). D) The relative luciferase activities in HEK293T cells co-transfected with a reporter containing WT or MUT 3'-UTR of MIG-7 and miR-520d-3p mimic or mimic control. Values are expressed as mean \pm SD (n=3). *p<0.05, **p<0.01

Conversely, the miR-520d-3p inhibitor led to increased lamellipodia and filopodia formation (Figure 5A).

Another key mediator of tumor VM formation is the PI3K/MMPs/Laminin-5 γ 2 pathway, which plays an essential role in promoting VM [29]. 143B and MG-63 cells overexpressing miR-520d-3p had decreased p-AKT, p-mTOR, Ln-5 γ 2', Ln-5 γ 2x levels, and increased Ln-5 γ 2 protein expression (Figure 5C). The decreased levels of MMP-2 and MMP-14 were confirmed by ELISA assays (Figure 5D). The opposite effects were shown in cells with miR-520d-3p low expression (Figures 5C, 5D). In addition, MIG-7 overexpression abolished these effects of miR-520d-3p, further indicating that miR-520d-3p exerts its function through regulating MIG-7 (Figures 5B, 5E, 5F). We also found that the addition of LY294002 inhibited activation of the PI3K/MMPs/Laminin-5 γ 2 signaling pathway as well as VM formation by OS cells (Supplementary Figures S2A, S2B, S2E). Furthermore, the effects, especially on promoting VM formation caused by miR-520d-3p inhibitor or MIG-7 in OS cells were found to be partially reversed by the LY294002 treatment (Supplementary Figures S2A–S2F), suggesting that miR-520d-3p/MIG-7 axis might regulate VM formation through the PI3K/MMPs/Laminin-5 γ 2 pathway.

miR-520d-3p inhibits OS xenograft growth, metastasis, and VM *in vivo* by targeting MIG-7. Overexpressing of miR-520d-3p inhibited tumor growth, whereas MIG-7 promoted it. Restoration of MIG-7 attenuated the inhibi-

tory effect of miR-520d-3p on tumor growth (Figures 6A, 6B). Consistently, tumor weights in these groups showed a similar trend (Figure 6C). Furthermore, while 100% of mice in the MIG-7 overexpression group formed lung metastases, fewer were detected in the miR-520d-3p group. Restoration of MIG-7 showed a higher frequency of metastasis by miR-520d-3p (Figures 6D, 6G). These metastatic frequencies may explain the survival times shown in Figure 6F. As expected, the levels of miR-520d-3p in LV-miR-520d-3p groups were significantly higher than those in the control-LV group (Figure 6E). IHC staining exhibited a raised level of MIG-7 in the MIG-7 vector group, whereas the LV-miR-520d-3p group showed lower level. Additionally, the MIG-7 vector efficiently rescued the MIG-7 protein level suppressed by miR-520d-3p (Figures 6G, 6H). Microscopically, OS cells showed a polygonal shape with large hyperchromatic nuclei. H&E staining revealed expanded necrosis in the miR-520d-3p overexpression group and reduced necrosis in the MIG-7 vector group. Both miR-520d-3p and MIG-7 overexpression groups exhibited less necrosis than miR-520d-3p overexpression alone (Figure 6G). IOD value demonstrated that the miR-520d-3p group had lower p-AKT, p-mTOR, MMP-2, and MMP-14 expression, whereas tumors from the MIG-7 vector group showed higher values. MIG-7 overexpression in the miR-520d-3p group reversed these values repressed by miR-520d-3p (Figure 6H). Similarly, VMD significantly declined in the miR-520d-3p group and increased in the

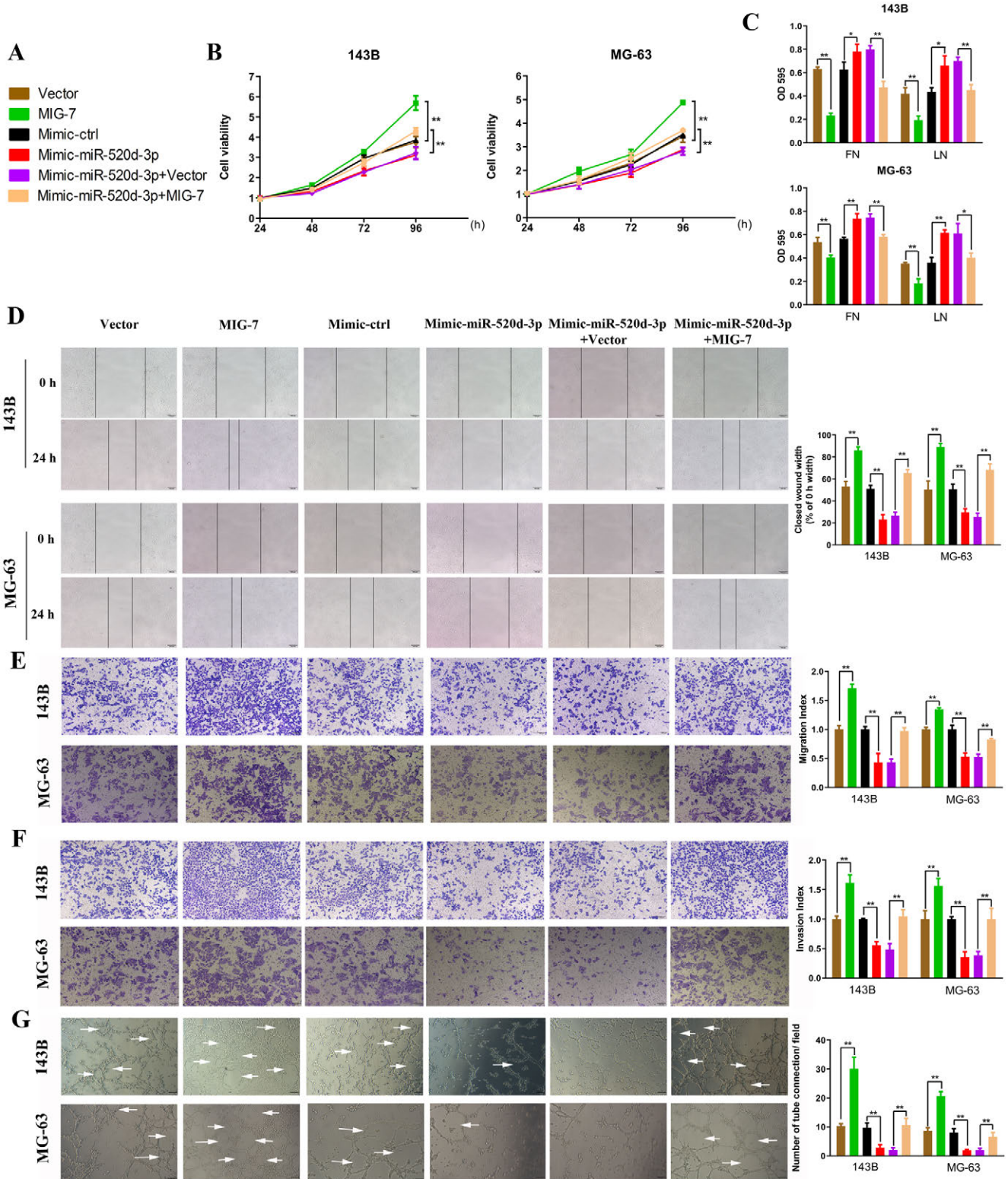


Figure 4. Restoration of MIG-7 rescued the miR-520d-3p-mediated inhibition of OS cell growth, adhesion, migration, invasion, and VM formation *in vitro*. A, B) CCK-8, cell adhesion (C), wound-healing (D), Transwell (E-F), tube formation (G) assays were performed to assess the effect of miR-520d-3p/MIG-7 axis on 143B and MG-63 cells transfected with miR-520d-3p mimic or co-transfected with miR-520d-3p mimic and MIG-7 construct. White arrows show VMs formed by OS cells. Scale bars: 100 μ m. Values are expressed as mean \pm SD (n=3). *p<0.05, **p<0.01

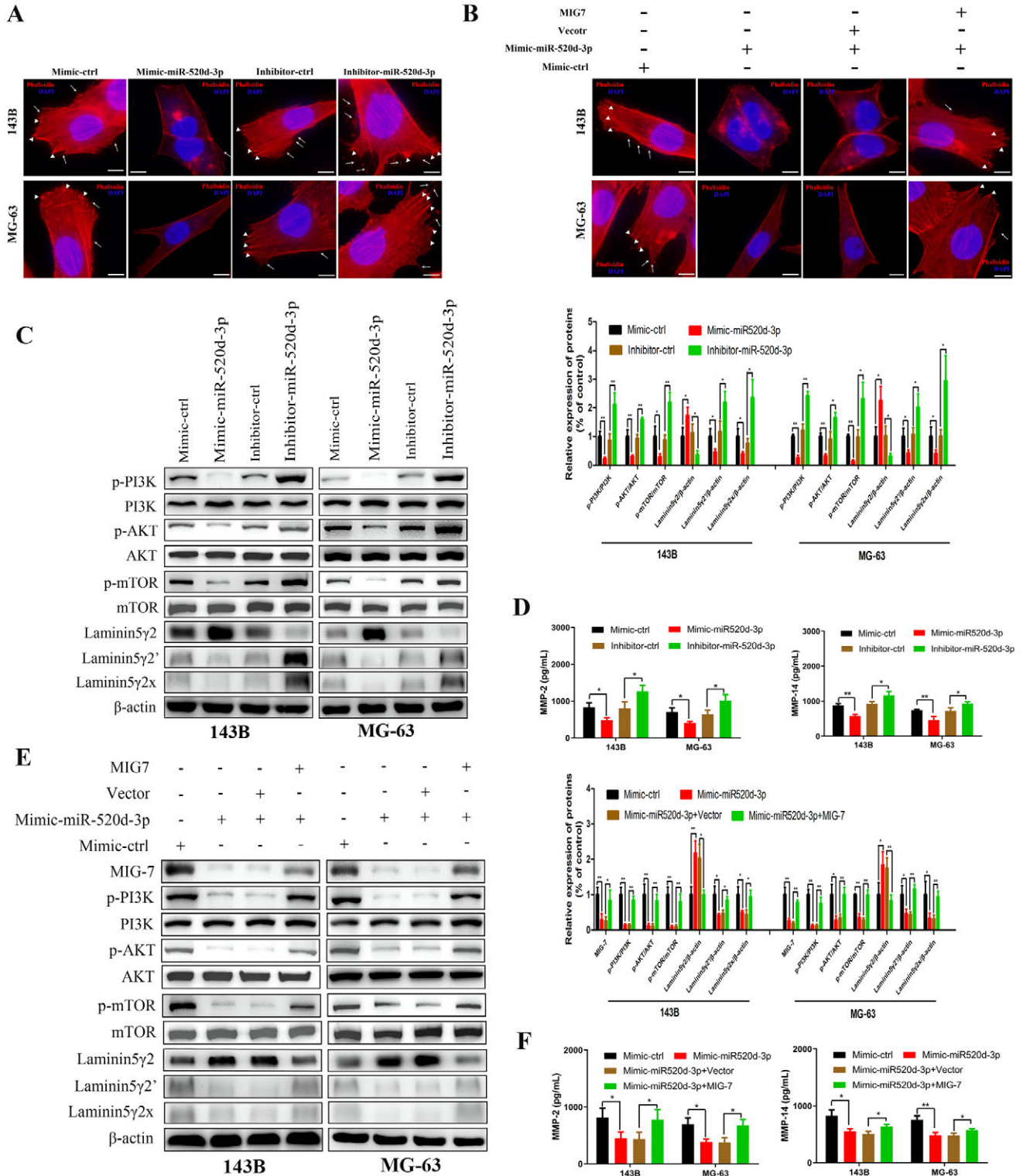


Figure 5. miR-520d-3p/MIG-7 regulates OS VM through modulating lamellipodia and filopodia formation and the PI3K/MMPs/Laminin-5γ2 pathway. A, B) Representative images of 143B and MG-63 cells transfected with miR-520d-3p mimic, inhibitor, or co-transfected with miR-520d-3p mimic and MIG-7 construct. White arrows indicate lamellipodia; white arrowheads indicate filopodia. Scale bars: 10 μm. C, E) 143B and MG-63 cells transfected with miR-520d-3p mimic, inhibitor, or co-transfected with miR-520d-3p mimic and MIG-7 construct were cultured on Matrigel. Protein was extracted as reported previously [38]. Protein levels were measured by western blot. D, F) Levels of MMP-2 and MMP-14 in the supernatant of cells were measured using ELISA assay. Values are expressed as mean ± SD (n=3). *p<0.05, **p<0.01

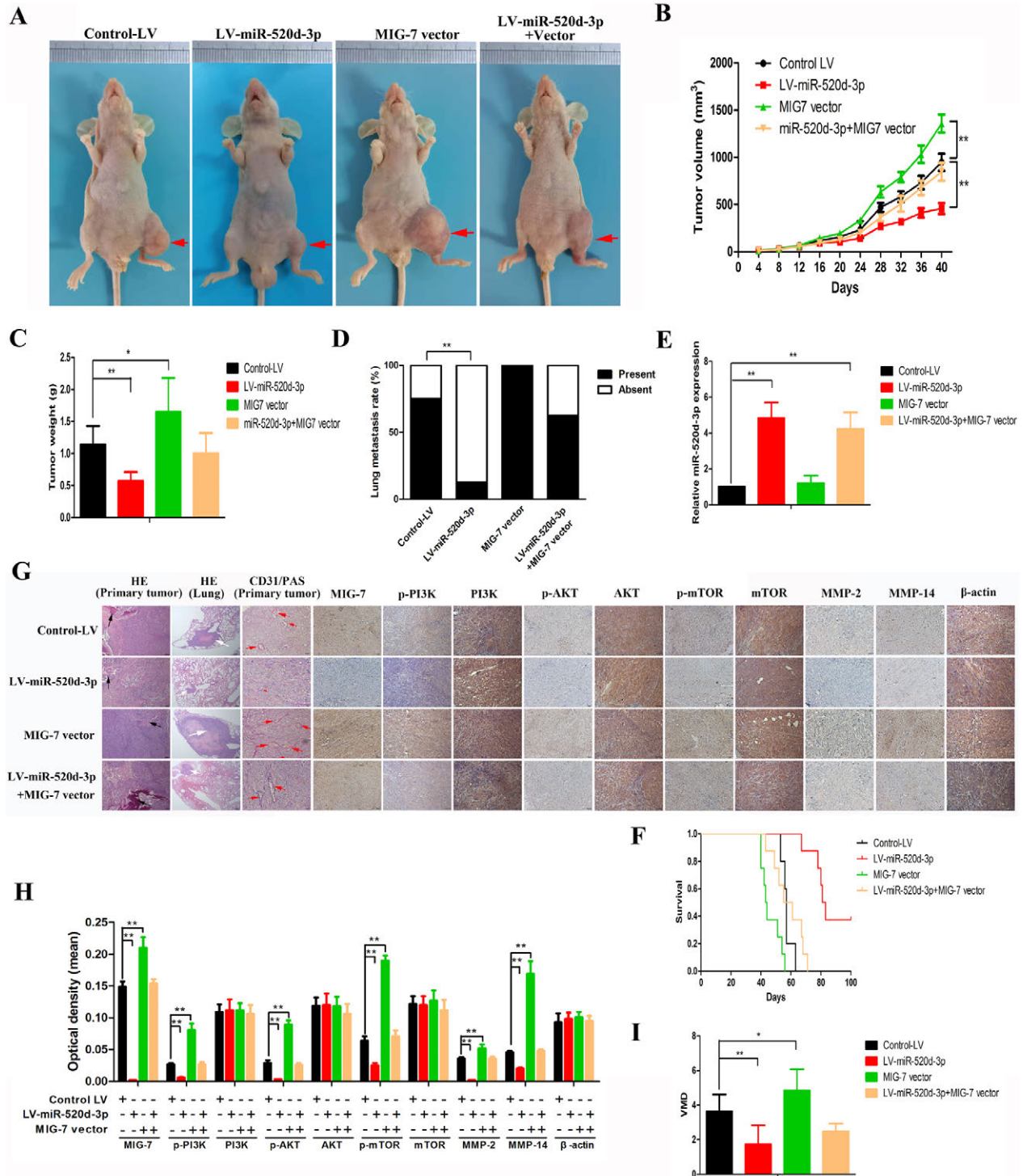


Figure 6. miR-520d-3p exhibits anti-OS, anti-metastasis, and anti-VM effects *in vivo* by targeting MIG-7. **A**) Representative mice from each group on day 40 after cell inoculation. Red arrows show enlarged local tumor formation in the left hindlimb at the site of injection. **B**) The growth curves of intratibial tumors were obtained every 4 days for a total of 10 measurements. Bar: SEM. **C**) Quantitative analysis of the tumor weights on day 40 post-implantation. **D**) Quantitative analysis of lung metastasis rate in each group. **E**) qRT-PCR analysis of miR-520d-3p levels in excised intratibial tumors from each group. **F**) Kaplan-Meier survival curves for each group of mice. **G**) Representative images of H&E and IHC staining (Scale bars: 100 μ m) for intratibial tumors and metastatic tumors in the lungs from each group. Black arrows show the bone cortex (Scale bars: 100 μ m). White arrows show lung micrometastases (Scale bars: 50 μ m). Red arrows show the VM channels (Scale bars: 20 μ m). **H**) The average IOD value of MIG-7, p-AKT, p-mTOR, MMP-2, and MMP-14 in intratibial tumors from each group. **I**) Quantitative analysis of VMD in each group. Values are expressed as mean \pm SD. * p <0.05, ** p <0.01

MIG-7 vector group. Overexpression of MIG-7 reversed the reduced VMD by miR-520d-3p. (Figure 6I). Taken together, these data suggested the anti-OS and anti-VM function of miR-520d-3p *in vivo* by targeting MIG-7.

Discussion

MIG-7 has been reported to be overexpressed in a variety of tumors and possessed pro-VM properties in aggressive malignancies [30, 31]. The oncogenic role of MIG-7 has been demonstrated in our previous study. However, further work is needed to uncover the mechanism underlying the MIG-7 mediated VM. First, a classical *in vitro* tube formation assay was employed to evaluate the ability of OS cells to form VM [32]. Different capacities in terms of VM formation were observed among these cells. MNNG/HOS cells that showed highly aggressive phenotypes also had superior abilities of VM formation, while 143B, MG-63, and U-2 OS cells exhibited intermediate VM-forming abilities. HOS and Saos-2 cells had poor VM formation capacities. No channels were observed in normal osteoblast cells on Matrigel. We next evaluated the level of the MIG-7 protein in these cell lines. The results indicated that OS cells with higher MIG-7 expression were more likely to form VM.

In the current study, we screened for miRNAs that can target MIG-7 and identified miR-520d-3p as a candidate. miR-520d-3p has been reported to be a tumor suppressor gene in different types of cancer [26, 27, 33]. However, its functions and regulation of MIG-7 in OS have not been elucidated. We found an opposite correlation between the level of miR-520d-3p and those of MIG-7 in these cell lines. This implies MIG-7, which plays an important role in VM formation in OS, is regulated by miR-520d-3p. Subsequently, MIG-7 was verified as a direct target of miR-520d-3p in two OS cell lines. We further confirmed that miR-520d-3p suppressed MIG-7 expression post-transcriptionally by binding to the 3'UTR of MIG-7 mRNA. *In vitro* functional assays demonstrated that miR-520d-3p overexpression inhibited OS cell proliferation, migration, invasion, VM formation, and promoted cell adhesion. Restoration of MIG-7 dramatically attenuated the anti-proliferative, anti-migratory, anti-VM effects of miR-520d-3p. It is commonly assumed that VM provides the requisite blood supply to fulfill rapid tumor growth [6]. Besides, the special structure of VM also increases the risk of tumor metastasis [8]. Indeed, *in vivo* CD31-PAS double staining, a gold standard for detecting the existence of VM [29] revealed that VM density was significantly decreased in tumors from the miR-520d-3p overexpression group in which tumors also exhibited suppressed growth, reduced lung metastasis rate, and prolonged survival time. Tumors from the MIG-7 overexpression group yielded an inverse effect. Additionally, MIG-7 overexpression reversed the anti-VM and anti-metastasis effect induced by miR-520d-3p. The present results suggested that these anti-OS effects of miR-520d-3p were mediated through targeting MIG-7.

The actin-based protrusions including lamellipodia and filopodia are essential for cell migration and their disruption resulted in reduced migratory and weakened VM ability [28]. Ehop-016 and ML141 are two potent small molecule inhibitors against lamellipodia or filopodia production, respectively [34, 35]. To confirm the contribution of lamellipodia and filopodia in OS cell mediated VM, the impacts of Ehop-016 and ML141 on VM formation were assessed (Supplementary Figures S3A, S3B). Since a loss in cell viability was not expected to affect the anti-VM effect of two inhibitors, we first tested OS cell viability in the presence of Ehop-016 or ML141. Ehop-016 at 1 μ M did not significantly affect cell viability. In line with those of previous studies [35], ML141 did not affect cell viability even at high concentrations. Non-toxic Ehop-016 and ML141 treatment with OS cells effectively disrupted VM channels and even more when used in combination, indicating the importance of their contributions to VM formation (Supplementary Figures S3A, S3B). In the present study, miR-520d-3p overexpression resulted in a dramatic decrease in lamellipodia and filopodia formation. MIG-7 overexpression rescued the disruptive effect of miR-520d-3p on lamellipodia and filopodia production. Likewise, MIG-7 knockdown suppressed the formation of these two protrusions (Supplementary Figures S4A–S4C). These results imply that lamellipodia and filopodia in OS cells were implicated in the MIG-7-dependent anti-VM function of miR-520d-3p.

A growing body of evidence has shown that the PI3K/MMPs/Ln-5 γ 2 signaling pathway mediates VM formation [29]. Laminin-5 (Ln-5) is a major component of the basement membrane and the cleavage of Ln-5 γ 2-chain plays a fundamental role in epithelial cell scattering [36]. Ln-5 γ 2-chain processing also took place during VM by aggressive tumor cells [15]. MMP-14 and MMP-2 overexpression synergistically promote proteolytic cleavage of Ln-5 γ 2-chain into fragments γ 2' and γ 2x [15]. These fragments have a promigratory effect and participate in VM formation [37]. Disturbed activation of the PI3K signaling pathway regulates the expression of MMP-14 and MMP-2, subsequently cleaving Ln-5 γ 2-chain and increasing the deposition of γ 2' and γ 2x chains in the extracellular matrix that ultimately contributes to the VM [38]. Inhibition of components in this signaling pathway could impair VM development [29]. In a xenograft nude mouse model, MIG-7 silencing led to dramatically reduced phosphorylation of AKT as well as MMP-14 [13]. In addition, increased Ln-5 γ 2 chain fragments were detected in colon carcinoma cells overexpressing MIG-7 cultured on Matrigel *in vitro* [12]. It has been shown that MMPs/Ln-5 γ 2 is the last step in the procession of VM. These findings led us to hypothesize that MIG-7 facilitates VM by activation of the PI3K/MMPs/Ln-5 γ 2 pathway.

In this study, western blot and IHC assays showed a decrease in PI3K activity after miR-520d-3p mimic transfection, as determined by phosphorylation of AKT and mTOR, a well-recognized approach for determining PI3K activa-

tion [39]. This result occurs concomitantly with a decreased amount of cleaved $\gamma 2'$ and $\gamma 2x$ and an increased proportion of uncleaved Ln-5 $\gamma 2$. Reduced levels of MMP-14 and MMP-2 were also found when the miR-520d-3p expression was upregulated. This is consistent with the increased *in vitro* adhesion ability of OS cells which may be due to the decreased levels of MMP-2 and MMP-14 the cells produce that can cleave Ln-5 $\gamma 2$ and degrade the extracellular matrix. Restoration of MIG-7 reversed the inactivation of the PI3K/AKT/mTOR pathway and its downstream effectors by miR-520d-3p. Consistently, MIG-7 knockdown blocked the PI3K/MMPs/Ln-5 $\gamma 2$ pathway in OS cells (Supplementary Figures S4A–S4C). Moreover, the effects of miR-520d-3p inhibitor or MIG-7 on the PI3K/MMPs/Ln-5 $\gamma 2$ pathway and VM channels could be abrogated by LY294002. Therefore, it can be inferred that miR-520d-3p directly regulated MIG-7 levels to modulate the PI3K/MMPs/Ln-5 $\gamma 2$ pathway in OS.

In summary, our work identified anti-VM and anti-metastasis role of miR-520d-3p in OS by targeting MIG-7 *in vitro* and *in vivo*. These findings provide a better understanding of the molecular events of tumorigenesis in OS and potential therapeutic target for OS treatment.

Supplementary information is available in the online version of the paper.

Acknowledgments: This work was supported by grants awarded by the National Natural Science Foundation of China (No. 81903851, 81873055) and the Jiangsu Province Natural Science Foundation (No. BK20191084).

References

- [1] FUCHS B, PRITCHARD DJ. Etiology of osteosarcoma. *Clin Orthop Relat Res* 2002; 397: 40–52. <https://doi.org/10.1097/00003086-200204000-00007>
- [2] FLETCHER CD, UNNI KK, MERTENS F. Pathology and genetics of tumours of soft tissue and bone. IARC Press, Lyon, 2002, p. 265. ISBN 92-832-2413-2
- [3] ALLISON DC, CARNEY SC, AHLMANN ER, HENDIFAR A, CHAWLA S et al. A meta-analysis of osteosarcoma outcomes in the modern medical era. *Sarcoma* 2012; 2012: 704872–704882. <https://doi.org/10.1155/2012/704872>
- [4] MILLER BJ, CRAM P, LYNCH CF, BUCKWALTER JA. Risk factors for metastatic disease at presentation with osteosarcoma: an analysis of the SEER database. *J Bone Joint Surg Am* 2013; 95: e89. <https://doi.org/10.2106/JBJS.L.01189>
- [5] FOLKMAN J. Role of angiogenesis in tumor growth and metastasis. *Semin Oncol* 2002; 29: 15–18. <https://doi.org/10.1053/sonc.2002.37263>
- [6] FERNÁNDEZ-CORTÉS M, DELGADO-BELLIDO D, OLIVER FJ. Vasculogenic mimicry: become an endothelial cell “but not so much”. *Front Oncol* 2019; 9: 803. <https://doi.org/10.3389/fonc.2019.00803>
- [7] SPILIOPOULOS K, PESCHOS D, BATISTATOU A, NTOUNTAS I, AGNANTIS N et al. Vasculogenic mimicry: lessons from melanocytic tumors. *In Vivo* 2015; 29: 309–317.
- [8] REN H, SHEN J, MAO X, ZHANG X, ZHOU P et al. Correlation between tumor vasculogenic mimicry and poor prognosis of human digestive cancer patients: a systematic review and meta-analysis. *Pathol Oncol Res* 2019; 25: 849–858. <https://doi.org/10.1007/s12253-018-0496-3>
- [9] REN K, YAO N, WANG G, TIAN L, MA J et al. Vasculogenic mimicry: a new prognostic sign of human osteosarcoma. *Hum Pathol* 2014; 45: 2120–2129. <https://doi.org/10.1016/j.humpath.2014.06.013>
- [10] CROUCH S, SPIDEL CS, LINDSEY JS. HGF and ligation of $\alpha v \beta 5$ integrin induce a novel, cancer cell-specific gene expression required for cell scattering. *Exp Cell Res* 2004; 292: 274–287. <https://doi.org/10.1016/j.yexcr.2003.09.016>
- [11] PHILLIPS TM, LINDSEY JS. Carcinoma cell-specific Mig-7: a new potential marker for circulating and migrating cancer cells. *Oncol Rep* 2005; 13: 37–44. <https://doi.org/10.3892/or.13.1.37>
- [12] PETTY AP, GARMAN KL, WINN VD, SPIDEL CM, LINDSEY JS. Overexpression of carcinoma and embryonic cytotrophoblast cell-specific Mig-7 induces invasion and vessel-like structure formation. *Am J Pathol* 2007; 170: 1763–1780. <https://doi.org/10.2353/ajpath.2007.060969>
- [13] PETTY AP, WRIGHT SE, REWERS-FELKINS KA, YENDERROZOS MA, VORDERSTRASSE BA et al. Targeting migration inducing gene-7 inhibits carcinoma cell invasion, early primary tumor growth, and stimulates monocyte oncolytic activity. *Mol Cancer Ther* 2009; 8: 2412–2423. <https://doi.org/10.1158/1535-7163.MCT-09-0186>
- [14] REN K, ZHANG J, GU X, WU S, SHI X et al. Migration-inducing gene-7 independently predicts poor prognosis of human osteosarcoma and is associated with vasculogenic mimicry. *Exp Cell Res* 2018; 369: 80–89. <https://doi.org/10.1016/j.yexcr.2018.05.008>
- [15] SEFTOR RE, SEFTOR EA, KOSHIKAWA N, MELTZER PS, GARDNER LM et al. Cooperative interactions of laminin 5 $\gamma 2$ chain, matrix metalloproteinase-2, and membrane type-1-matrix/metalloproteinase are required for mimicry of embryonic vasculogenesis by aggressive melanoma. *Cancer Res* 2001; 61: 6322–6327.
- [16] ZHU W, SUN W, ZHANG J, LIU Z, LI X et al. Norcantharidin enhances TIMP-2 anti-vasculogenic mimicry activity for human gallbladder cancers through downregulating MMP-2 and MT1-MMP. *Int J Oncol* 2015; 46: 627–640. <https://doi.org/10.3892/ijo.2014.2753>
- [17] YANG J, LIAO Y, MAI D, XIE P, QIANG Y et al. Tumor vasculogenic mimicry predicts poor prognosis in cancer patients: a meta-analysis. *Angiogenesis* 2016; 19: 191–200. <https://doi.org/10.1007/s10456-016-9500-2>
- [18] CHEN J, CHEN S, ZHUO L, ZHU Y, ZHENG H. Regulation of cancer stem cell properties, angiogenesis, and vasculogenic mimicry by miR-450a-5p/SOX2 axis in colorectal cancer. *Cell Death Dis* 2020; 11: 1–13. <https://doi.org/10.1038/s41419-020-2361-z>
- [19] SONG Y, MU L, HAN X, LI Q, DONG B et al. MicroRNA-9 inhibits vasculogenic mimicry of glioma cell lines by suppressing Stathmin expression. *J Neurooncol* 2013; 115: 381–390. <https://doi.org/10.1007/s11060-013-1245-9>

- [20] ZHAO N, SUN H, SUN B, ZHU D, ZHAO X et al. miR-27a-3p suppresses tumor metastasis and VM by down-regulating VE-cadherin expression and inhibiting EMT: an essential role for Twist-1 in HCC. *Sci Rep* 2016; 6: 1–16. <https://doi.org/10.1038/srep23091>
- [21] BARTEL DP. MicroRNAs: genomics, biogenesis, mechanism, and function. *Cell* 2004; 116: 281–297. [https://doi.org/10.1016/s0092-8674\(04\)00045-5](https://doi.org/10.1016/s0092-8674(04)00045-5)
- [22] RAM KUMAR RM, BORO A, FUCHS B. Involvement and clinical aspects of microRNA in osteosarcoma. *Int J Mol Sci* 2016; 17: 877. <https://doi.org/10.3390/ijms17060877>
- [23] LI X, LIU W, LIU J, WANG W, ZHANG S et al. Expression of angiopoietins in central nervous system hemangioblastomas is associated with cyst formation. *Neurosci Lett* 2017; 639: 120–125. <https://doi.org/10.1016/j.neulet.2016.12.066>
- [24] BETEL D, KOPPAL A, AGIUS P, SANDER C, LESLIE C. Comprehensive modeling of microRNA targets predicts functional non-conserved and non-canonical sites. *Genome Biol* 2010; 11: 1–14. <https://doi.org/10.1186/gb-2010-11-8-r90>
- [25] KERTESZ M, IOVINO N, UNNERSTALL U, GAUL U, SEGAL E. The role of site accessibility in microRNA target recognition. *Nat Genet* 2007; 39: 1278–1284. <https://doi.org/10.1038/ng2135>
- [26] XIANG Y, HUANG Y, SUN H, PAN Y, WU M et al. Dereglulation of miR-520d-3p promotes hepatocellular carcinoma development via lncRNA MIAT regulation and EPHA2 signaling activation. *Biomed Pharmacother* 2019; 109: 1630–1639. <https://doi.org/10.1016/j.biopha.2018.11.014>
- [27] REN Z, YANG T, DING J, LIU W, MENG X et al. MiR-520d-3p antitumor activity in human breast cancer via post-transcriptional regulation of spindle and kinetochore associated 2 expression. *Am J Transl Res* 2018; 10: 1097–1108.
- [28] MAES H, VAN EYGEN S, KRYSKO D, VANDENABEELE P, NYS K et al. BNIP3 supports melanoma cell migration and vasculogenic mimicry by orchestrating the actin cytoskeleton. *Cell Death Dis* 2014; 5: e1127. <https://doi.org/10.1038/cddis.2014.94>
- [29] LUO Q, WANG J, ZHAO W, PENG Z, LIU X et al. Vasculogenic mimicry in carcinogenesis and clinical applications. *J Hematol Oncol* 2020; 13: 19. <https://doi.org/10.1186/s13045-020-00858-6>
- [30] ROBERTSON GP. Mig-7 linked to vasculogenic mimicry. *Am J Pathol* 2007; 170: 1454–1456. <https://doi.org/10.2353/ajpath.2007.070127>
- [31] HO M, HUNG S, LIANG C, LIANG S. Recombinant viral capsid protein VP1 suppresses lung cancer metastasis by inhibiting COX-2/PGE2 and MIG-7. *Oncotarget* 2014; 5: 3931–3943. <https://doi.org/10.18632/oncotarget.2040>
- [32] FRANCESCONE 3RD R, FAIBISH M, SHAO R. A Matrigel-based tube formation assay to assess the vasculogenic activity of tumor cells. *Journal of Visualized Experiments: JoVE* 2011; 55: e3040. <https://doi.org/10.3791/3040>
- [33] LI R, YUAN W, MEI W, YANG K, CHEN Z. MicroRNA 520d-3p inhibits gastric cancer cell proliferation, migration, and invasion by downregulating EphA2 expression. *Mol Cell Biochem* 2014; 396: 295–305. <https://doi.org/10.1007/s11010-014-2164-6>
- [34] MONTALVO-ORTIZ BL, CASTILLO-PICHARDO L, HERNÁNDEZ E, HUMPHRIES-BICKLEY T, MOTA-PEYNADO AD et al. Characterization of EHOp-016, novel small molecule inhibitor of Rac GTPase. *J Biol Chem* 2012; 287: 13228–13238. <https://doi.org/10.1074/jbc.M111.334524>
- [35] SURVILADZE Z, WALLER A, STROUSE JJ, BOLOGA C, URSU O et al. A potent and selective inhibitor of Cdc42 GTPase. *Probe Reports from the NIH Molecular Libraries Program*. 2010. NBK51965
- [36] GIANNELLI G, FALK-MARZILLIER J, SCHIRALDI O, STETLER-STEVENSON WG, QUARANTA V. Induction of cell migration by matrix metalloproteinase-2 cleavage of laminin-5. *Science* 1997; 277: 225–228. <https://doi.org/10.1126/science.277.5323.225>
- [37] KOSHIKAWA N, GIANNELLI G, CIRULLI V, MIYAZAKI K, QUARANTA V. Role of cell surface metalloproteinase MT1-MMP in epithelial cell migration over laminin-5. *The J Cell Biol* 2000; 148: 615–624. <https://doi.org/10.1083/jcb.148.3.615>
- [38] HESS AR, SEFTOR EA, SEFTOR RE, HENDRIX MJ. Phosphoinositide 3-kinase regulates membrane Type 1-matrix metalloproteinase (MMP) and MMP-2 activity during melanoma cell vasculogenic mimicry. *Cancer Res* 2003; 63: 4757–4762.
- [39] VARA JÁF, CASADO E, DE CASTRO J, CEJAS P, BELDA-INIESTA C et al. PI3K/Akt signalling pathway and cancer. *Cancer Treat Rev* 2004; 30: 193–204. <https://doi.org/10.1016/j.ctrv.2003.07.007>

https://doi.org/10.4149/neo_2022_211128N1683

miR-520d-3p/MIG-7 axis regulates vasculogenic mimicry formation and metastasis in osteosarcoma

Nan YAO^{1,2,*}, Jing ZHOU^{1,2}, Jie SONG^{1,2}, Yantao JIANG³, Jian ZHANG^{1,2}

Supplementary Information

Supplementary materials and methods

Cell treatment. To investigate involvement of PI3K/AKT pathway in miR-520d-3p/MIG-7 mediated VM formation, LY294002 (20 μ M, Sigma-Aldrich, St. Louis, St. Louis, MO), a specific PI3K inhibitor, was applied to 143B and MG-63 cells transfected with miR-520d-3p inhibitor or MIG-7 vector.

Cell proliferation assay. The cell proliferation of 143B and MG-63 cells after treatment with different concentration of EHop-016 (HY-12810, MedChemExpress, NJ, USA) and ML141 (HY-12755, MedChemExpress) were examined using CCK-8 assay.

In vitro VM assay. The effect of EHop-016 and ML141 on the vasculogenic activity of 143B and MG-63 cells were assessed by the Matrigel-based VM assay.

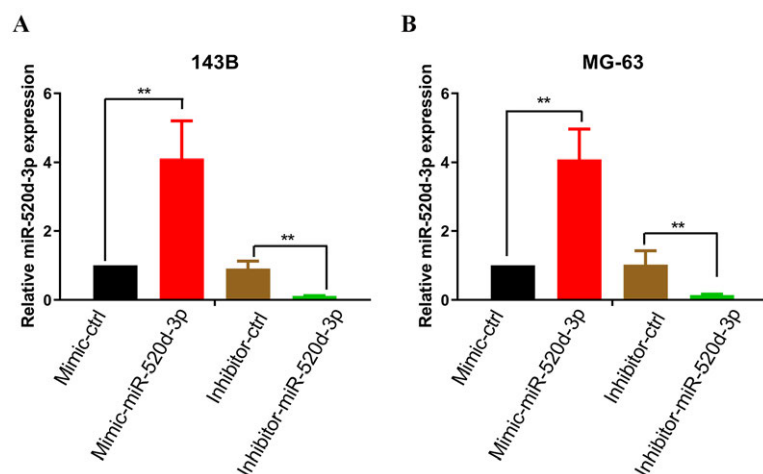
Construction of MIG-7-shRNA lentiviral vector and cell infection. The small hairpin RNA (shRNA) sequence that targeted MIG-7 gene (Accession DQ080207) was synthesized and cloned into the GV493 lentivirus expression plasmid (GeneChem, Shanghai, China). The shRNA sequencers were as follows: shMIG-7: 5'-GCAAGTA-CAGGGCAGAATTTTC-3'. The scramble negative control sequence was 5'-TTCTCCGAACGTGTCACGT-3'. Viral particle was produced by co-transfection of 293T cells with packaging helper plasmids (pHelper 1.0 and 2.0 vectors) and cloned DNAs using Lipofectamine 2000. After the Lenti-MIG-7-sh was transduced into the 143B and MG-63 cells,

stable cell lines were obtained with puromycin treatment and denoted as shMIG-7 cells. The cells transduced with Lenti-NC are denoted as scramble cells.

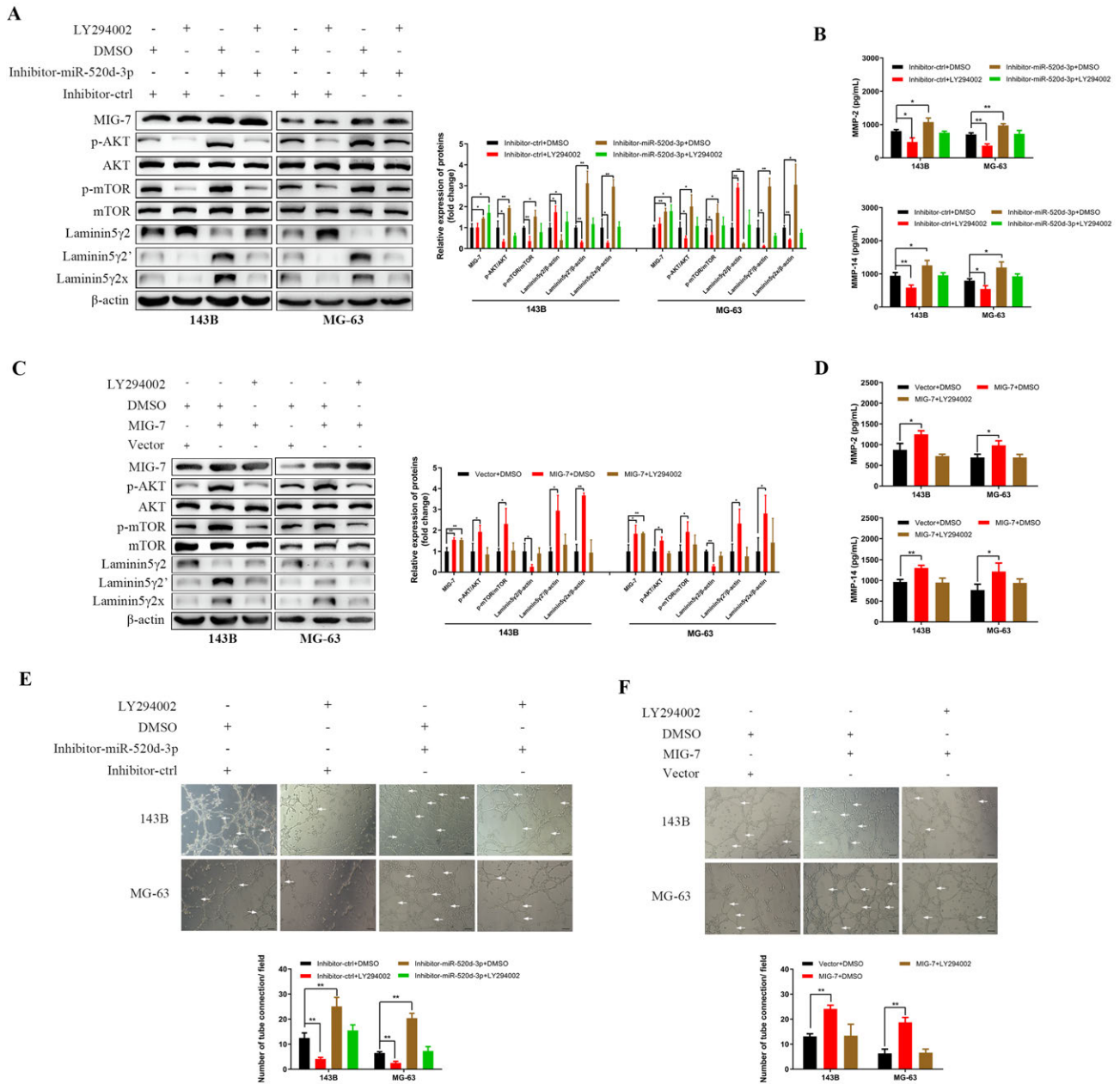
Phalloidin staining. After stained with rhodamine-phalloidin (5783, R&D system), the cells were counterstained with DAPI and imaged using a microscopy (Axio Primo Vert A1).

Western blot analysis. Cells were collected and lysed in RIPA (Beyotime) supplemented with proteinase inhibitor cocktail (Solarbio). An equal amount (50 μ g) of the protein samples were separated by SDS-PAGE and incubated with the primary antibodies against MIG-7 (bs-5781R, 1:1000, Bioss), PI3K (ab180967, 1:2000, Abcam), p-PI3K (ab182651, 1:1000, Abcam), AKT (4691T, 1:2000, CST), p-AKT (4060T, 1:2000, CST), mTOR (2983T, 1:1000, CST), p-mTOR (5536T, 1:1000, CST), laminin 5 γ 2 and its fragments (MAB19562, 1:1000, Chemicon) at 4 $^{\circ}$ C overnight, followed by incubating with horseradish peroxidase-labeled secondary antibody (SA00001-1, SA00001-2, Proteintech). β -actin (66009-1-Ig, 1:2000, Proteintech) was used as an internal control. The bands were visualized by ECL kit (180-5001, Tanon) and quantized by IPP software.

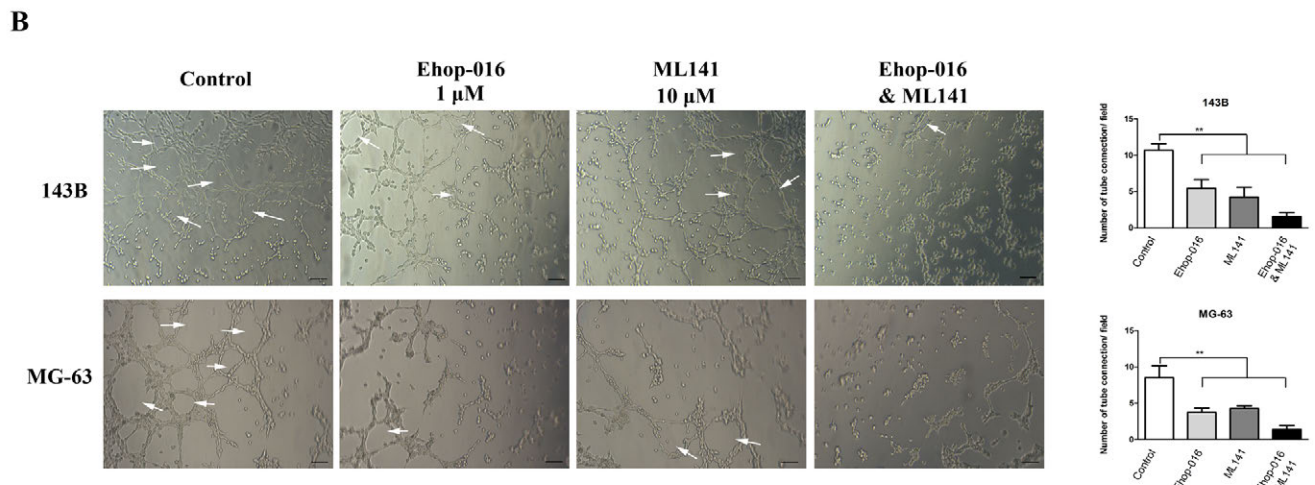
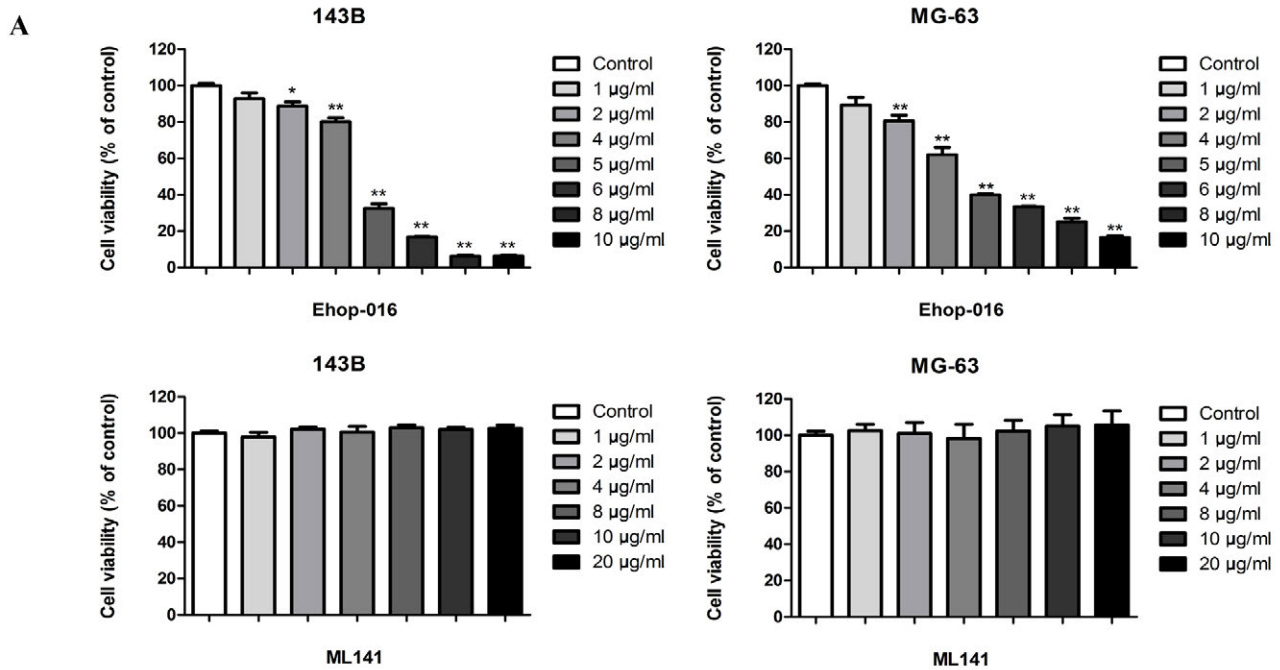
ELISA assay. The levels of MMP-2 (EK1M02-96, Multi-Sciences) and MMP-14 (HM10943, Bioswamp) in cell culture supernatant were determined using ELISA kits according to the manufacturing instruction.



Supplementary Figure S1. qRT-PCR analysis of miR-520d-3p expression levels in 143B (A) and MG-63 cells (B) transfected with miR-520d-3p mimic, inhibitor, or negative control.



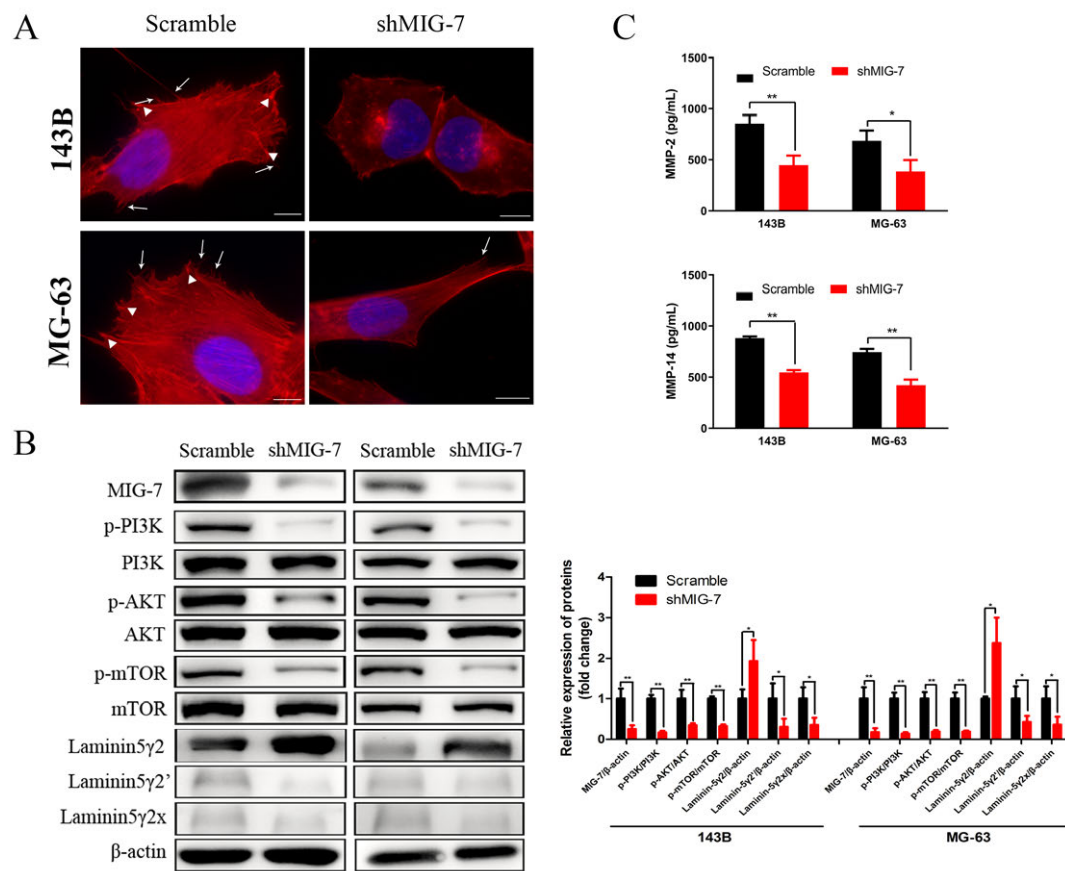
Supplementary Figure S2. Effects of LY294002 on PI3K/MMPs/Ln-5γ2 pathway and VM formation in OS cells. A) 143B and MG-63 cells transfected with inhibitor control plus DMSO, inhibitor control plus LY294002, miR-520d-3p inhibitor plus DMSO or miR-520d-3p inhibitor plus LY294002 were cultured on Matrigel. Protein was extracted as reported previously [38]. Protein levels were measured by western blot. Levels of MMP-2 and MMP-14 in the supernatant of these cells were measured using ELISA assay (B). C) 143B and MG-63 cells transfected with empty vector plus DMSO, MIG-7 vector plus DMSO or MIG-7 vector plus LY294002 were cultured on Matrigel. Protein was extracted as reported previously [38]. Protein levels were measured by western blot. Levels of MMP-2 and MMP-14 in the supernatant of these cells were measured using ELISA assay (D). E, F) Representative images of VM formation ability of miR-520d-3p inhibitor- or MIG-7- transfected 143B and MG-63 cells after LY294002 treatment. White arrows show VMs formed by OS cells. Scale bars: 10 μm. Values are expressed as mean±SD (n=3). *p<0.05, **p<0.01



Supplementary Figure S3. A) The anti-proliferative effects of EHop-016 and ML141 in 143B and MG-63 cells. 143B and MG-63 cells were treated with different concentrations of EHop-016 and ML141 for 24 h. cell viability was measured by CCK-8 assay. B) Representative images of control versus EHop-016 (1 µM) and/or ML141 (10 µM) treated 143B or MG-63 cells grown on Matrigel. White arrows show VMs formed by OS cells. Values are expressed as mean±SD (n=3). Scale bars: 100 µm. *p<0.05, **p<0.01

Supplementary Table S1. Primer for qPCR.

Genes (<i>Homo sapiens</i>)	Primers	Sequences
miR-520d-3p	Forward	5'-CGCGAAAGTGCTTCTCTTTG-3'
	Reverse	5'-AGTGCAGGGTCCGAGGTATT-3'
U6	Forward	5'-CTCGCTTCGGCAGCAC-3'
	Reverse	5'-AACGCTTACGAAATTTGCGT-3'



Supplementary Figure S4. MIG-7 knockdown inhibits lamellipodia and filopodia formation and PI3K/MMPs/Laminin-5 γ 2 pathway. A) 143B and MG-63 cells transfected with lentiviral vectors expressing MIG-7-specific shRNA or a negative control were incubated with the Phalloidin- rhodamine and the nuclear dye DAPI. Representative images of scramble control versus shMIG-7 transduced cells are shown. White arrows indicate lamellipodia; White arrowheads indicate filopodia. Scale bars: 10 μ m. B) Cells were cultured on Matrigel. Protein levels were measured by western blot. (C) Levels of MMP-2 and MMP-14 in the supernatant of cells were measured by ELISA assay. Values are expressed as mean \pm SD (n=3). *p<0.05, **p<0.01